ELSEVIER

Chemical Engineering Journal 85 (2002) 41–51

Chemical Engineering Journal

www.elsevier.com/locate/cej

Effect of catalytic surface curvature on the chemical performance with defect structures

Z.U.A. Warsi*, John F. Belena

Department of Aerospace Engineering, Mississippi State University, Mississippi State, MS 39762, USA

Received 30 March 2000; received in revised form 10 January 2001; accepted 10 January 2001

Abstract

This paper describes the steady-state chemical performance of catalytic surfaces of similar constitution but of varied global curvature exposed to two distinct chemical species which are allowed to adsorb, desorb, diffuse and react on the surface. The surface reactions are modeled to include the presence of defect structures which exist due to lattice faults and/or foreign material on the surface. Flat, circular and elliptical cylindrical surfaces are examined with similar desorption and reaction rates at the defect sites so as to evaluate the role of surface curvature on the steady-state behavior of the surface species concentrations. The methodology described here is applicable to generally curved surfaces referred to general curvilinear coordinates generated numerically to conform with the surface shapes. The continuum reaction–diffusion models transformed to the general curvilinear coordinates are solved numerically by the line successive-over-relaxation (SOR) method. Numerical results show that decreasing the surface curvature enhances the chemical process in the presence of surface defects.

Keywords: Adsorption; Desorption; Catalyst activation; Numerical analysis

1. Introduction

The subject of heterogeneous catalysis with chemical reaction kinetics has been of much interest due to its applicability in space flight structures and in atomic reactors. From a practical view point, almost all catalytic reactors contain active surfaces which involve lattice faults and/or foreign material on the surfaces. Though the problem is essentially of molecular origin some very important results can be obtained by performing an analysis from a continuum view point. The continuum approach was applied by Grinstein et al. [1] and we refer to their work for the definitions of varied terms, the nondimensionalization [1] scheme, and to their results obtained for a flat catalytic surface.

In heterogeneous catalysis, the catalyst is commonly found in the form of a porous grain, ranging from powder size to large-sized particles. As the size of the catalyst particle increases a point is reached at which the catalytic reaction will produce products in the interior of the grain faster than diffusion can carry them away. As the particle size is further enlarged, the catalytic reaction is confined to the outer layers of the particle and the catalytic activity becomes proportional to the external surface of the particle [2]. In the manufacture of a catalyst pellet with curved surfaces, surface roughness is necessarily introduced through surface dislocations, kinks and step defects in the lattice that are required to form a curved surface. The heterogeneous chemistry is greatly influenced by the geometrical structure of the catalyst, which may have a vital effect on catalyst selectivity and the surface defects like kinks, steps and terraces can influence the catalytic reaction significantly [3–6].

With surface irregularities or defects playing a major role in influencing the catalytic activity of the external surface of the manufactured catalyst particle we designed flat, elliptical and circular surfaces with surface defects in accordance with the method of Grinstein et al. [1]. The existence of surface defects usually affects the adsorption and desorption rates of the surface. The adsorption rates can be designed to vary in the presence of surface defects by using nominal adsorption intensities α_{i0} in the place of nominal desorption intensities β_{i0} in Section 2.3 of this work. Letting the presence of the surface defects modify the surface desorption rate only is a sufficient condition to allow for the investigation of the role surface curvature on a global scale plays in the catalytic activity of the surface.

* Corresponding author. Tel.: +1-662-325-7293.
E-mail address: warsi@ae.msstate.edu (Z.U.A. Warsi).

[1] The scheme for nondimensionalization is the same as detailed in [1]. The only exception is that ξ and η of [1] are denoted as ω and χ, respectively. All lengths have been nondimensionalized by using $1/\sqrt{f_1}$ as the length scale.

1385-8947/02/$ – see front matter
PII: S1385-8947(01)00139-5

Nomenclature

Dimensional variables

C	thermal transfer rate coefficient of the bulk medium
D_i	diffusion coefficient of chemical species; $D_{i0}\exp\lfloor -E_{\mathrm{D}}^{i}/kT\rfloor$
$E_{\mathrm{A}}^{(\iota)}$	activation energy for surface adsorption for chemical species
$E_{\mathrm{D}}^{(i)}$	activation energy for surface diffusion for chemical species
$E_{\mathrm{DS}}^{(i)}$	activation energy for surface desorption for chemical species
$E_{\mathrm{R}}^{(\iota)}$	activation energy for reaction on surface
f_i	inverse of length scale squared based on chemical species; $s_{i0}/(D_{j0}u_{j0})$
H	specific enthalpy of formation of the reaction product
J_i	surface incident mass flux of chemical species
k	Boltzmann constant
K	reaction rate constant; $K_0(\eta,\zeta,\xi)\exp\lfloor -E_{\mathrm{R}}/kT\rfloor$
L_i	chemical loss rate of species
m_i	particle mass of chemical species
$\boldsymbol{n}$	surface outward unit normal vector
n_i	number density of chemical species
Q_i	chemical production rate of species
s_i	surface incident adsorbed mass flux of chemical species; $\mu_i J_i$; $(s_{i0}=\mu_{i0}J_i)$
T	local temperature at the surface; $T(\eta_0,\zeta,\xi)$
T_0	bulk temperature
u_i	surface concentration of chemical species
$\boldsymbol{v}$	fluid velocity vector
$\boldsymbol{v}_{\mathrm{di}}$	diffusion velocity vector of chemical species
X, Y, Z	rectangular Cartesian coordinates
Γ_i	desorption rate constant of chemical species; $\gamma_i(\eta_0,\zeta,\xi)\exp\lfloor -E_{\mathrm{PS}}^{(i)}/kT\rfloor$
i	adsorption coefficient of chemical species; $\mu_{i0}\exp\lfloor -E_{\mathrm{A}}^{(i)}/kT\rfloor$

Nondimensional variables

v_i	relative surface concentration of chemical species; u_i/u_{i0}
x, y, z	nondimensional rectangular Cartesian coordinates
β_i	nondimensional desorption rate for chemical species; $u_{i0}\gamma_i(\eta_0,\zeta,\xi)/s_{i0}$
χ	ratio of length scales squared; f_2/f_1
ε_{R}	normalized activation energy for reaction on the surface; $E_{\mathrm{R}}/(kT_0)$
$\varepsilon_{\mathrm{A}}^{(i)}$	normalized activation energy for surface adsorption for chemical species; $E_{\mathrm{A}}^{(i)}/(kT_0)$
$\varepsilon_{\mathrm{D}}^{(i)}$	normalized activation energy for surface diffusion for chemical species; $E_{\mathrm{D}}^{(i)}/(kT_0)$
$\varepsilon_{\mathrm{DS}}^{(i)}$	normalized activation energy for surface desorption for chemical species; $E_{\mathrm{DS}}^{(i)}/(kT_0)$
η_0	surface $\eta=\eta_0=$ const. on which the general coordinates are ζ, ξ
η, ζ, ξ	general curvilinear coordinates
φ	catalyst effectiveness factor
κ_i	nondimensional reaction rate constant for chemical species; $K_0(\eta_0,\zeta,\xi)u_{j0}/(D_{i0}f_i)\{(i,j):(1,2),(2,1)\}$
τ	nondimensional surface temperature T/T_0
ω	nondimensional specific heat of formation; $Hu_{10}u_{20}K_0(\eta_0,\zeta,\xi)/(CT_0)$
Δ_2	surface Beltramian; Eq. (A.7)
∇^2	Laplacian

In this paper, we study the steady-state chemical performance of active curved surfaces from a continuum point of view, embedded in a three-dimensional Euclidean space. As in [1], the active surface is exposed to two chemical species which adsorb, desorb, diffuse and react on the surface. The heterogeneous surface is modeled through the inclusion of arbitrarily distributed surface defects. These defects serve to locally enhance or diminish the processes of adsorption, desorption, chemical reactivity and heat transfer. In this regard, refer also to Serri et al. [7], and Cukier [8].

The main aim of this paper is to investigate the role of surface curvature on the steady-state chemical performance of active catalytic surfaces with surface defects. In addition to the calculations for flat surfaces as given in [1], the surfaces of circular and elliptic cylinders are considered with the same "random" defects. The analysis technique of this paper is also applicable to surfaces of arbitrary shapes because of the universal technique of numerical coordinate generation as developed by Thompson et al. [9], and Warsi [10]. The main idea here is to generate the coordinates in arbitrary surfaces through a system of partial differential equations as reported in [10] and then solve the transformed diffusion–reaction equations on these coordinates. The resulting equations have been solved numerically by the line successive-over-relaxation (SOR) method.

To clearly see the effects of curvature on the products of the physicochemical processes, the fluid velocity was set to zero. Also for simplicity, it has been assumed that the resultant product molecules of reaction desorb immediately after their production. From the comparison of the results discussed in Section 3, we see that in the presence of surface defects the curvature of the catalytic surface enhances the activity of reaction.

2. Analysis

From an analytic continuum standpoint, surface kinetic phenomenon is described by the continuity equations for the species and the total energy equation. Referring to Oran and Boris [11], the continuity equation of the ith species is

$$\frac{\partial n_i}{\partial t} + \operatorname{div}(n_i \boldsymbol{v}) + \operatorname{div}(n_i \boldsymbol{v}_{\mathrm{di}}) = Q_i - L_i n_i \tag{1a}$$

where n_i is the number density of the ith species. Denoting by m_i the molecular or particle mass of the ith species, the equation for the concentration $u_i = n_i m_i$ is obtained from Eq. (1a) as

$$\frac{\partial u_i}{\partial t} + \operatorname{div}(u_i \boldsymbol{v}) + \operatorname{div}(u_i \boldsymbol{v}_{\mathrm{di}}) = Q_i m_i - L_i u_i \tag{1b}$$

The total energy equation is

$$\frac{\partial E}{\partial t} + \operatorname{div}(E\boldsymbol{v}) - \operatorname{div}(\boldsymbol{T}\cdot\boldsymbol{v}) + \operatorname{div}(\boldsymbol{q} + \boldsymbol{q}_{\mathrm{r}}) = \boldsymbol{v}\cdot\sum_i \mathrm{m}_i \boldsymbol{f}_i + \sum_i \boldsymbol{v}_{\mathrm{di}} m_i \boldsymbol{f}_{\mathrm{r}} \tag{2}$$

where $\boldsymbol{T}$ is the Stokes' stress tensor and $\boldsymbol{f}_i$ the body force vector per unit mass associated with the ith species.

Since u_i is the concentration, the diffusion velocity $\boldsymbol{v}_{\mathrm{di}}$ is proportional to the gradient of u_i. On dimensional consideration, the relation between $\boldsymbol{v}_{\mathrm{di}}$ and u_i is

$$u_i \boldsymbol{v}_{\mathrm{di}} = -D_i \operatorname{grad} u_i \tag{3}$$

For steady-state and in the absence of fluid flow while using Eq. (3) in Eq. (1b), the conservation equation simplifies to

$$\operatorname{div}(D_i \operatorname{grad} u_i) + Q_i m_i - L_i u_i = 0 \tag{4a}$$

or

$$D_i \nabla^2 u_i + (\operatorname{grad} D_i)\cdot(\operatorname{grad} u_i) + Q_i m_i - L_i u_i = 0 \tag{4b}$$

Under the above stated conditions and also neglecting the body force terms, the energy equation, Eq. (2), reduces to

$$\operatorname{div} \boldsymbol{q} = 0 \tag{5}$$

At this stage, it must be noted that the Laplacian ∇^2 appearing in Eq. (4b) is in general three-dimensional, i.e.

$$\nabla^2 = \partial_{XX} + \partial_{YY} + \partial_{ZZ}$$

where X, Y, Z are the rectangular Cartesian coordinates.

The purpose of this paper is to compute the concentration functions u_i on a curved surface. As in [1], we take two species so that the two equations from Eq. (4b) are

$$D_1 \nabla^2 u_1 + (\operatorname{grad} D_1)\cdot(\operatorname{grad} u_1) + Q_1 m_1 - L_1 u_1 = 0 \tag{6}$$

$$D_2 \nabla^2 u_2 + (\operatorname{grad} D_2)\cdot(\operatorname{grad} u_2) + Q_2 m_2 - L_2 u_2 = 0 \tag{7}$$

We now nondimensionalize Eqs. (6) and (7) by following the scheme used by Grinstein et al. (refer to Nomenclature) but for simplicity keep the same notation for the Laplacian and the gradient operators. Thus, in Eqs. (6) and (7) replacing ∇^2 by $f_1\nabla^2$ and grad by $\sqrt{f_1}\operatorname{grad}$, we get

$$f_1 D_i \nabla^2 u_i + f_1(\operatorname{grad} D_i)\cdot(\operatorname{grad} u_i) = L_i u_i - Q_i m_i; \quad i = 1, 2$$

Using

$$v_i = \frac{u_i}{u_{i0}}, \qquad D_i = D_{i0}\exp\left(\frac{-\varepsilon_{\mathrm{D}}^{(i)}}{\tau}\right)$$

we get

$$\nabla^2 v_i = \varepsilon_{\mathrm{D}}^{(i)} \operatorname{grad}\left(\frac{1}{\tau}\right)\cdot\operatorname{grad} v_i + \exp\left[\frac{\varepsilon_{\mathrm{D}}^{(i)}}{\varepsilon}\right]\frac{(L_i u_{i0} v_i - Q_i m_i)}{f_1 u_{i0} D_{i0}} \tag{8}$$

where $i = 1, 2$. Transforming the Laplacian and the gradient to general coordinates ξ, η, ζ (refer to Appendix A), taking η as the normal coordinate on the surface $\eta = \eta_0 = \text{const.}$, and then evaluating each term of Eq. (8) on the surface, we get the following two equations:

At $\eta = \eta_0$

$$\Delta_2 v_1 = \varepsilon_{\mathrm{D}}^{(1)} \operatorname{grad}\left(\frac{1}{\tau}\right)\cdot\operatorname{grad} v_1 - \left(\frac{\partial^2 v_1}{\partial\eta^2} + \frac{1}{2G_2}\frac{\partial G_2}{\partial\eta}\frac{\partial v_1}{\partial\eta}\right) + \frac{L_1}{f_1 D_{10}}\exp\left[\frac{\varepsilon_{\mathrm{D}}^{(1)}}{\tau}\right] v_1 - \frac{Q_1 m_i}{f_1 u_{10} D_{10}}\exp\left[\frac{\varepsilon_{\mathrm{D}}^{(1)}}{\tau}\right] \tag{9}$$

$$\Delta_2 v_2 = \varepsilon_{\mathrm{D}}^{(2)} \operatorname{grad}\left(\frac{1}{\tau}\right)\cdot\operatorname{grad} v_2 - \left(\frac{\partial^2 v_2}{\partial\eta^2} + \frac{1}{2G_2}\frac{\partial G_2}{\partial\eta}\frac{\partial v_2}{\partial\eta}\right) + \left(\frac{L_2}{f_1 D_{20}} v_2 - \chi\frac{Q_2 m_2}{f_2 D_{20} u_{20}}\right)\exp\left[\frac{\varepsilon_{\mathrm{D}}^{(2)}}{\tau}\right] \tag{10}$$

where Δ_2 is the surface Beltramian as defined in (A.6) and the expressions for $\Delta_2 v_1$, $\Delta_2 v_2$ are as given in Eq. (A.7), and $\chi = f_2/f_1$. It must be noted that the second terms on the right hand sides of Eqs. (9) and (10) are formed of the normal derivatives of v_1 and v_2 at the surface and they, in general, are not zero. In the following, we have merged these terms in the modeling of the terms on the right hand side to coincide with the form of the equations as those given in [1].

2.1. Modeling

At the surface $\eta = \eta_0$, we have modeled the terms to be consistent from a physical standpoint as follows:

$$\frac{L_1}{f_1 D_{10}} = \kappa_1 v_2 \exp\left[\frac{-\varepsilon_{\mathrm{R}}}{\tau}\right] + \beta_1 \exp\left[\frac{-\varepsilon_{\mathrm{DS}}^{(1)}}{\tau}\right] \tag{11a}$$

$$\frac{L_2}{f_1 D_{20}} = \kappa_2 v_1 \exp\left[\frac{-\varepsilon_{\mathrm{R}}}{\tau}\right] + \chi\beta_2 \exp\left[\frac{-\varepsilon_{\mathrm{DS}}^{(2)}}{\tau}\right] \tag{11b}$$

$$\frac{Q_1}{f_1 u_{10} D_{10}} + \left(\frac{\partial^2 v_1}{\partial \eta^2} + \frac{1}{2G_2}\frac{\partial G_2}{\partial \eta}\frac{\partial v_1}{\partial \eta}\right) \exp\left[\frac{-\varepsilon_{\mathrm{D}}^{(1)}}{\tau}\right] = \exp\left[\frac{-\varepsilon_{\mathrm{A}}^{(1)}}{\tau}\right] \exp(-v_1) \tag{11c}$$

$$\frac{\chi Q_2 m_2}{f_2 D_{20} u_{20}} + \left(\frac{\partial^2 v_2}{\partial \eta^2} + \frac{1}{2G_2}\frac{\partial G_2}{\partial \eta}\frac{\partial v_2}{\partial \eta}\right) \exp\left[\frac{-\varepsilon_{\mathrm{D}}^{(2)}}{\tau}\right] = \chi \exp\left[\frac{-\varepsilon_{\mathrm{A}}^{(2)}}{\tau}\right] \exp(-v_2) \tag{11d}$$

Substitution of the modeled terms (11) in Eqs. (9) and (10) yield the equations

$$\Delta_2 v_1 = \varepsilon_{\mathrm{D}}^{(1)} \operatorname{grad}\left(\frac{1}{\tau}\right) \cdot \operatorname{grad} v_1 + \kappa_1 \exp\left[\frac{(\varepsilon_{\mathrm{D}}^{(1)} - \varepsilon_{\mathrm{R}})}{\tau}\right] v_1 v_2 - \exp\left[\frac{\varepsilon_{\mathrm{D}}^{(1)} - \varepsilon_{\mathrm{A}}^{(1)}}{\tau}\right] \times \left\{\exp(-v_1) - \beta_1 v_1 \exp\left[\frac{(\varepsilon_{\mathrm{A}}^{(1)} - \varepsilon_{\mathrm{DS}}^{(1)})}{\tau}\right]\right\} \tag{12}$$

$$\Delta_2 v_2 = \varepsilon_{\mathrm{D}}^{(2)} \operatorname{grad}\left(\frac{1}{\tau}\right) \cdot \operatorname{grad} v_2 + \kappa_2 \exp\left[\frac{(\varepsilon_{\mathrm{D}}^{(2)} - \varepsilon_{\mathrm{R}})}{\tau}\right] v_1 v_2 \chi \exp\left[\frac{\varepsilon_{\mathrm{D}}^{(2)} - \varepsilon_{\mathrm{A}}^{(2)}}{\tau}\right] \times \left\{\exp(-v_2) - \beta_2 v_2 \exp\left[\frac{(\varepsilon_{\mathrm{A}}^{(2)} - \varepsilon_{\mathrm{DS}}^{(2)})}{\tau}\right]\right\} \tag{13}$$

Further, assuming no defects at the boundaries of the catalytic surface, we impose the constant flux boundary conditions

$$\Delta_2 v_1 = 0, \quad \Delta_2 v_2 = 0 \tag{14}$$

at the boundaries. We now model the heat flux vector $\boldsymbol{q}$ as

$$\boldsymbol{q} = -k \operatorname{grad} T + \rho H \boldsymbol{v}_{\mathrm{di}}$$

where k is the conductivity (J/m s K), H the heat of formation per unit mass (J/kg), and $\rho = m_3 n_3$ the density of the species generated leaving the surface. Thus, taking

$$k\nabla^2 T = C(T - T_0) \tag{15a}$$

and

$$\operatorname{div}(\rho H \boldsymbol{v}_{\mathrm{di}}) = KHu_1 u_2 \tag{15b}$$

the energy equation, Eq. (5), yields a nondimensional algebraic equation

$$\omega v_1 v_2 \exp\left[\frac{-\varepsilon_{\mathrm{R}}}{\tau}\right] - (\tau - 1) = 0 \tag{16}$$

For brevity denoting the right-hand side terms of Eqs. (12) and (13) by R_1 and R_2, we have

$$\Delta_2 v_1 = R_1$$
$$\Delta_2 v_2 = R_2$$

Using the expression for the Beltramian's Eq. (A.7) with $\Delta_2\zeta = 0$ and $\Delta_2\xi = 0$, we have

$$g_{11} v_{1\zeta\zeta} - 2g_{13} v_{1\zeta\xi} + g_{33} v_{1\xi\xi} = G_2 R_1 \tag{17a}$$

$$g_{11} v_{2\zeta\zeta} - 2g_{13} v_{2\zeta\xi} + g_{33} v_{2\xi\xi} = G_2 R_2 \tag{17b}$$

where a variable subscript denotes a partial derivative. It must be stated here that the Beltramian of the coordinates, viz. $\Delta_2\zeta$ and $\Delta_2\xi$ are the coordinate control functions (for details, refer to [10]) and they are completely user specified functions to attain a desired distribution of coordinates in a given surface. The coordinate generating equations [10] with $\Delta_2\zeta = 0$ and $\Delta_2\xi = 0$ are given in vector form as

$$g_{11}\boldsymbol{r}_{\zeta\zeta} - 2g_{13}\boldsymbol{r}_{\zeta\xi} + g_{33}\boldsymbol{r}_{\xi\xi} = G_2(k_I + k_{II})\boldsymbol{n} \tag{18}$$

where $\boldsymbol{r} = (x, y, x)$ and $k_I + k_{II}$ is the sum of the principal curvatures at a point on the surface. If the equation of the surface is given as $F(x, y, x) = 0$ then the sum $k_I + k_{II}$ can be expressed as a function of x, y, z (refer to [10] for details.) Thus, Eq. (18) forms a set of three coupled simultaneous quasilinear equations for the determination of the coordinates $\boldsymbol{r}(\zeta, \xi) = (x(\zeta, \xi), y(\zeta, \xi), z(\zeta, \xi))$. For simply connected domains, only the boundary data $\boldsymbol{r}(\zeta_0, \xi), \boldsymbol{r}(\zeta_1, \xi), \boldsymbol{r}(\zeta, \xi_0), \boldsymbol{r}(\zeta, \xi_1)$ (where $\zeta_0 \le \zeta \le \zeta_1$ and $\xi_0 \le \xi \le \xi_1$) are needed, which are the Dirichlet boundary conditions. It must be noted that one does not have to prescribe the parametric values ζ_0, ζ_1, ξ_0, and ξ_1, since the solution of Eq. (18) is essentially expressed in the logical or integer space as $\boldsymbol{r}(K, I)$.

2.2. Numerical methodology

The first step in the numerical implementation is to solve Eq. (18) for $\boldsymbol{r}(K, I)$ when the surface has been specified. Noting that

$$g_{11} = x_\xi^2 + y_\xi^2 + z_\xi^2, \quad g_{13} = x_\xi x_\zeta + y_\xi y_\zeta + z_\xi z_\zeta,$$
$$g_{33} = x_\zeta^2 + y_\zeta^2 + z_\zeta^2, \quad G_2 = g_{11}g_{33} - (g_{13})^2$$

we approximate Eq. (18) by using the central difference approximation for both the first and the second partial derivatives with respect to ζ and ξ. Using integers K and I for ζ and ξ, respectively, the SOR method to solve the system of equations implies that for any dependent variable $\Psi = (x, y, z)$,

$$\Psi^{(p)}(K, I) = \omega\hat{\Psi}^{(p)}(K, I) + (1 - \omega)\Psi^{(p-1)}(K, I) \tag{19a}$$

where ω is the acceleration parameter ($1 < \omega < 2$) and p the iteration counter. The values of $\hat{\Psi}$ are obtained by solving

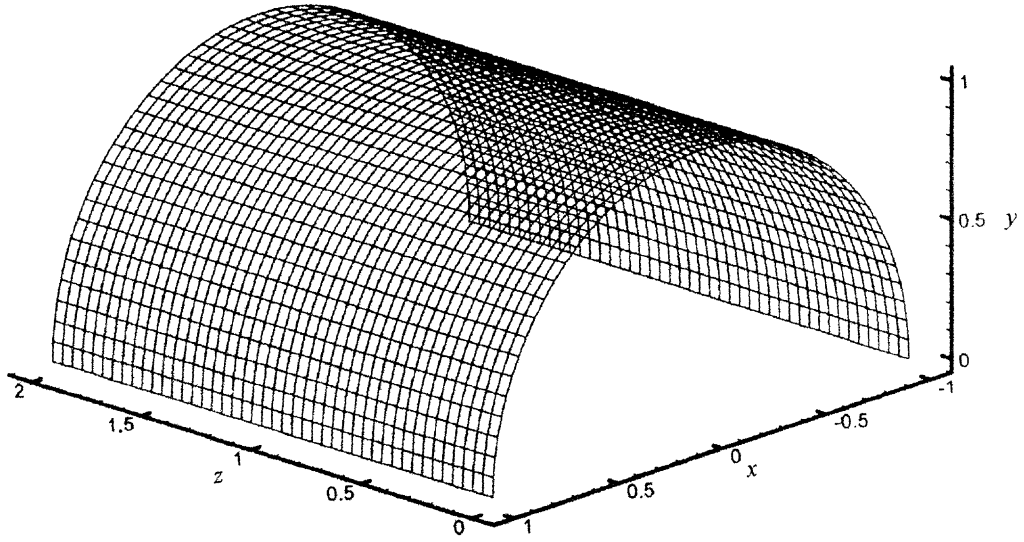

Fig. 1. Generated coordinate curves on the upper half of a circular cylinder.

the tridiagonal system

$$E\hat{\Psi}^{(p)}(K, I) + B\hat{\Psi}^{(p)}(K+1, I) + A\Psi^{(p)}(K-1, I) = -F(K, I) - C\Psi^{(p)}(K, I-1) - D\Psi^{(p-1)}(K, I+1) \quad (19b)$$

where the coefficients *E, B, A*, etc. depend on the values of the dependent variables, i.e. *x, y, z*, as available from the previous iteration. Figs. 1 and 2 show the coordinate lines ζ and ξ on a circular cylinder of radius 1 and elliptic cylinder of semi major and semi minor axes 2:1, respectively.

For each geometry, the values of $g_{11}(K, I)$, $g_{13}(K, I)$, $g_{33}(K, I)$ and $G_2(K, I)$, are stored in a data file. These values are then used in solving Eq. (17) by using the same algorithm. The boundary values for solving Eq. (17) are obtained by solving the nonlinear algebraic system $R_1 = 0$, $R_2 = 0$ according to the requirement of constant flux boundary conditions (Eq. (14)).

2.3. Modeling of the defect functions

The nondimensional desorption rate for chemical species β_i are dependent on the desorption coefficients γ_i which are considered to be functions of the surface coordinates, i.e. $\gamma_i(\zeta, \xi)$. The desorption defect functions $\beta_i(\zeta, \xi)$ should either be specified or modeled. Following the formulation of [1], the desorption defect functions $\beta_i(\zeta, \xi)$ have been modeled as follows:

$$\beta_i(\zeta, \xi) = \beta_{i0}\left[\sum_{j=1}^{n} D_j(\zeta, \xi)\right], \quad i = 1, 2, \quad (20)$$

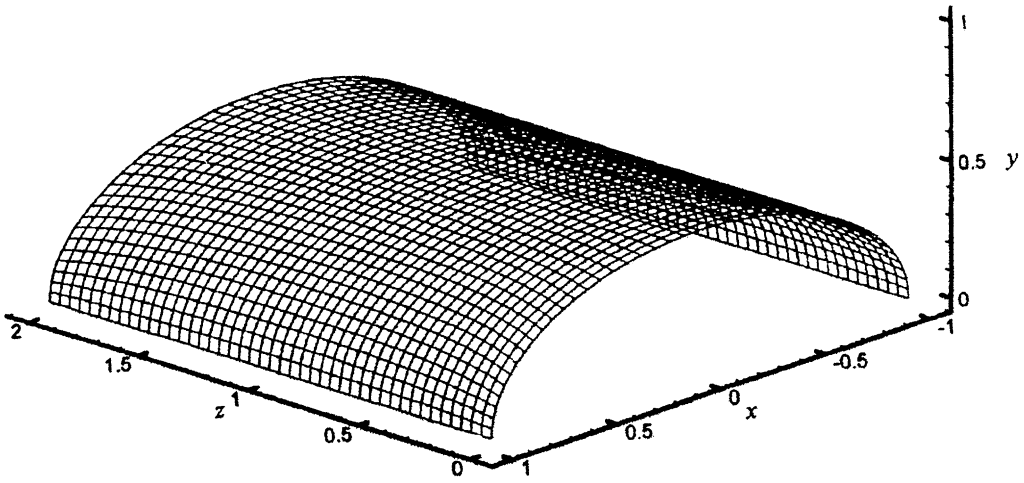

Fig. 2. Generated coordinate curves on the upper half of an elliptic cylinder.

Table 1
Parameters defining the defect functions D_j

j	ζ_j	ξ_j	σ_j	δ_j	θ_j (°)
1	0.7727	0.5909	0.0625	0.2650	135
2	0.4773	1.4091	0.0625	0.0156	90
3	0.9773	1.1591	0.0625	0.0880	45
4	1.4545	0.7726	0.0625	0.2500	90

where β_{i0} are constants specifying the nominal desorption intensities and n is the number of surface defects. For demonstration, we have taken $n = 4$ and selected $\beta_{10} = 3$ and $\beta_{20} = 10$. The n defect functions D_j have been taken as

$$D_j(\zeta, \xi) = \frac{1}{n} - \exp\left[-\left(\frac{\zeta_j^0}{\sigma_j}\right)^2\right] w(\xi_j^0, a_j, \delta_j)$$

where

$$\zeta_j^0 = (\zeta - \zeta_j)\cos\theta_j + (\xi - \xi_j)\sin\theta_j \tag{21}$$

$$\xi_j^0 = -(\zeta - \zeta_j)\sin\theta_j + (\xi - \xi_j)\cos\theta_j$$

$$\begin{aligned}\omega(\zeta_j^0, \sigma_j, \delta_j) &= \exp\left[-\left\{(\zeta_j^0 - \delta_j)/\sigma_j\right\}^2\right]; \quad \zeta_j^0 \geq \delta_j \\ &= 1; \qquad\qquad\qquad\qquad -\delta_j < \zeta_j^0 < \delta_j \\ &= \exp\left[-\left\{(\zeta_j^0 + \delta_j)/\sigma_j\right\}^2\right]; \ \zeta_j^0 \leq -\delta_j\end{aligned}$$

Each surface defect is modeled for maximum trapping at the core where the center of the "line defect" is at the point (ζ_j, ξ_j) and its orientation with respect to the ζ-coordinate line is given by the angle θ_j. Each defect is prescribed by a width and a length parameter σ_j and δ_j, respectively. The values of the parameters σ_j, δ_j, and θ_j used in the modeling are given in Table 1.

Based on the preceding modeling the defect functions $\beta_1(\zeta, \xi)$ and $\beta_2(\zeta, \xi)$ used on all surfaces are shown in Figs. 3 and 4. It must be mentioned here that the parameteric values of ζ and ξ appearing in Eq. (20) have been taken as

$$\zeta = 2\frac{(K-1)}{(K_{\max}-1)}, \qquad \xi = 2\frac{(I-1)}{(L_{\max}-1)}$$

where

$$1 \leq K \leq K_{\max}, \ 1 \leq I \leq L_{\max}, \text{ and } K_{\max} = 45, \ L_{\mathrm{MAX}} = 45.$$

3. Discussion of numerical results

To understand the effect of surface curvature on the steady-state chemical concentrations produced on surfaces with low surface coverages, we have solved the nondimensional Eqs. (12) and (13) on flat, circular, and elliptical surfaces. In all cases, the surfaces were subjected to the same heterogenous chemical environment. The desorptive properties of each surface was modeled as discussed in Section 2.3 so that in each case the same distribution of random defects as function of the generated coordinates was used. For simplicity, the temperature dependent effects were neglected and an isotropic reaction rate constant was chosen. Further, the diffusion and adsorption coefficients were taken as constants. Thus, the following data was chosen to

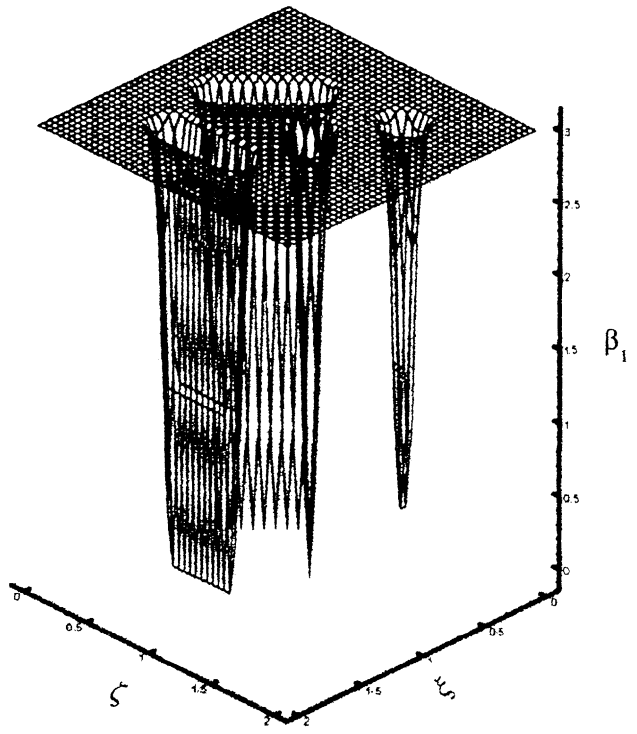

Fig. 3. Distribution of the desorption defect function β_1 (refer to Section 2.3).

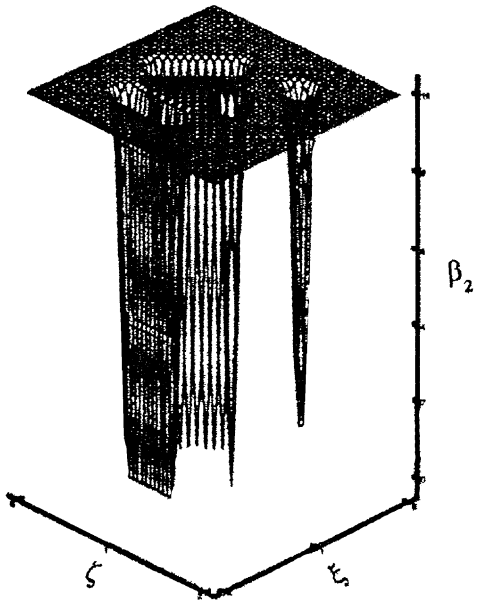

Fig. 4. Distribution of the desorption defect function β_2 (refer to Section 2.3).

calculate the concentration functions v_1 and v_2 on all surfaces.

$$\tau = 1, \quad \varepsilon_R = 0, \quad \varepsilon_D^{(i)} = \varepsilon_{DS}^{(i)} = 0$$

$$\beta_{10} = 3.0, \quad \beta_{20} = 10.0, \quad \kappa_1 = \kappa_2 = 2000$$

$$\chi = 10.0, \quad H = 0, \quad \frac{\gamma_2}{\gamma_1} = \frac{100}{3}, \quad \frac{D_{20}}{D_{10}} = 1$$

$$\frac{s_2}{s_1} = \frac{10u_{20}}{u_{10}}$$

Figs. 5–7 illustrate the results obtained for the concentrations v_1, v_2 and $k_2 v_1 v_2$. A comparative summary of v_1, v_2, and $k_2 v_1 v_2$ for various surfaces is given in Tables 2–4. The tables provide the change of the maximum and minimum values as compared to the flat surface as a reference surface of curvature ∞. From Tables 2–4, we conclude that the maximum concentration v_2 increases by about 8% and the minimum concentration v_1 decreases by about 7.2% for the cylindrical surfaces in comparison to the flat surface.

The general theory of chemical reactor analysis and design of heterogeneous catalytic systems relies on the

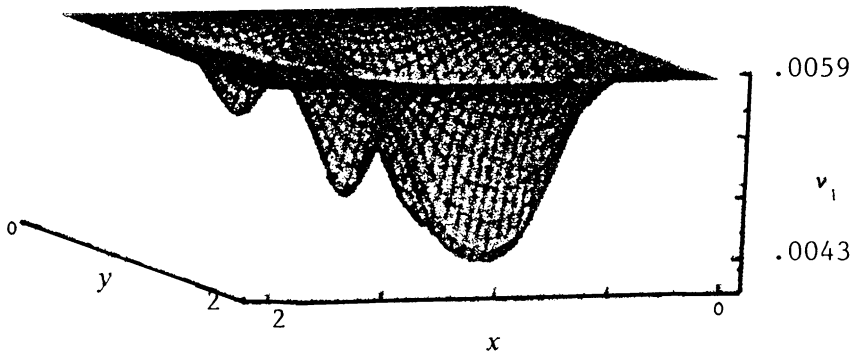

a. Flat Surface : Exposed Area 4

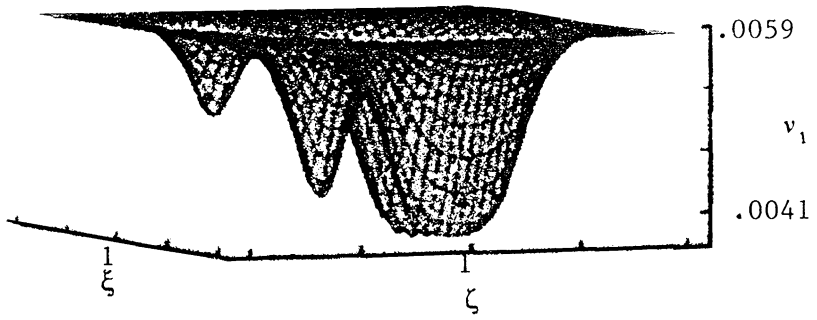

b. Elliptical Surface : (Semi major axis - 1. Semi minor axis -0.5) Exposed Area 3.162 pi

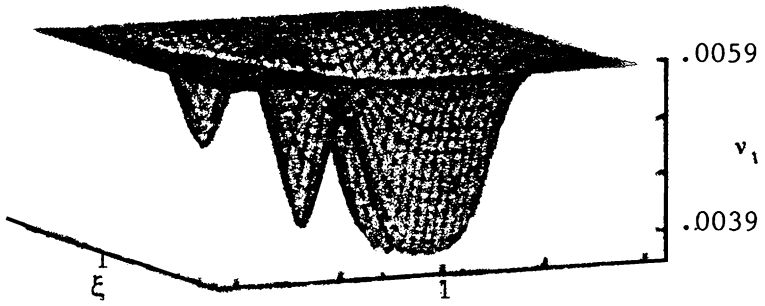

c. Cylindrical Surface : (Radius -1) Exposed Area 2 pi

Fig. 5. Concentration profiles of v_1 for various surfaces (refer to data in Section 4).

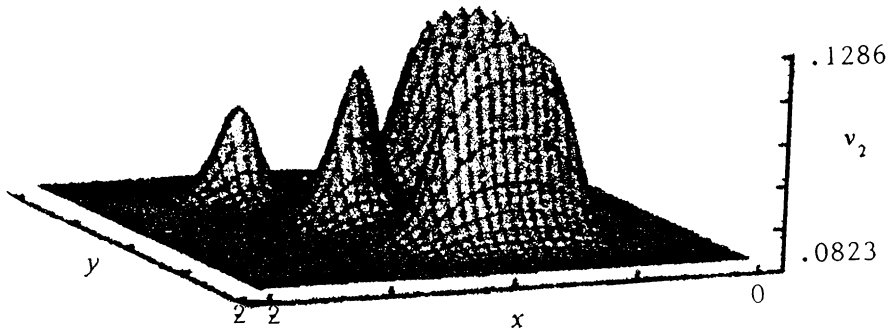

a. Flat Surface : Exposed Area 4

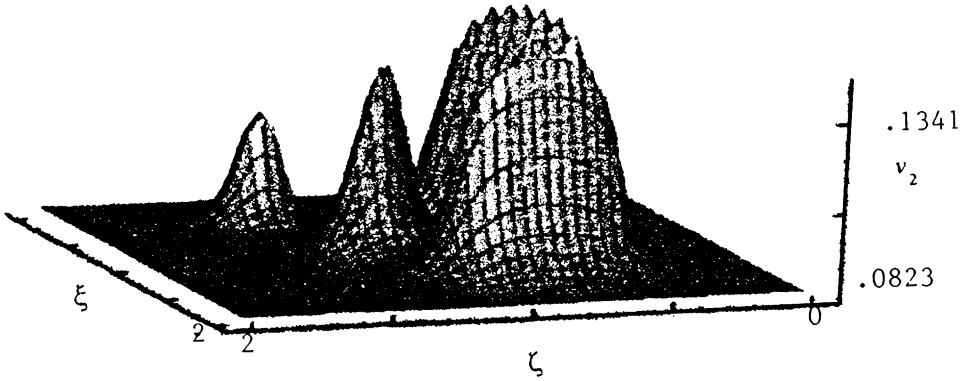

b. Elliptical Surface : (Semi major axis - 1. Semi minor axis -0.5)
Exposed Area 3.162 pi

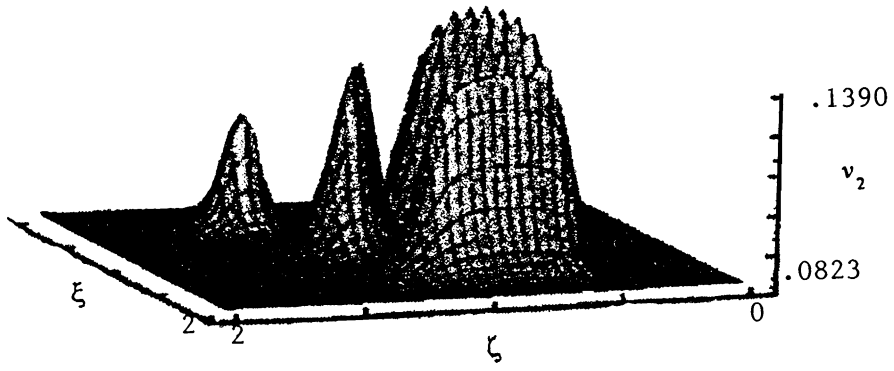

c. Cylindrical Surface : (Radius -1)
Exposed Area 2 pi

Fig. 6. Concentration profiles of v_2 for various surfaces (refer to data in Section 4).

catalyst effectiveness factor φ. In this regard, see Paterson and Creswell [12], and Ramachandran et al. [13].

$$\phi = \frac{\text{actual reaction rate}}{\text{rate as predicted by intrinsic kinetics}}$$

In practice, knowledge of φ at every point of a reactor is vital to its analysis and design because most chemical reactors do not operate where the intrinsic kinetics are applicable. The φ approach satisfies the need for estimating the actual reaction rates given the intrinsic kinetics and operating conditions within the reactor. Many chemical reactors use packed beds of catalyst particles, hence, the φ factor is also used to define the net chemical activity of a catalyst particle. From Tables 2–4, we see that a catalyst surface with

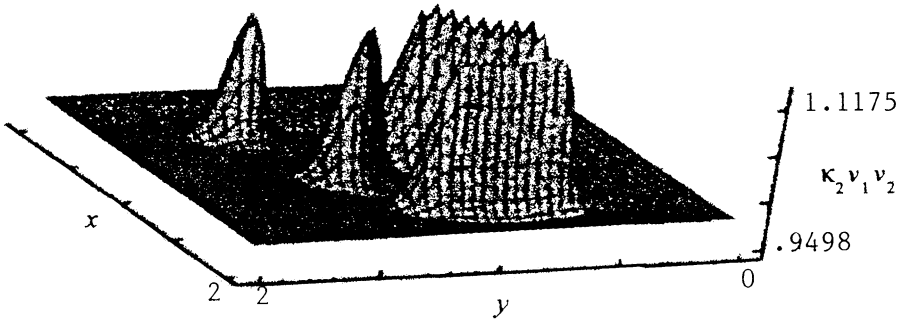

a. Flat Surface : Exposed Area 4

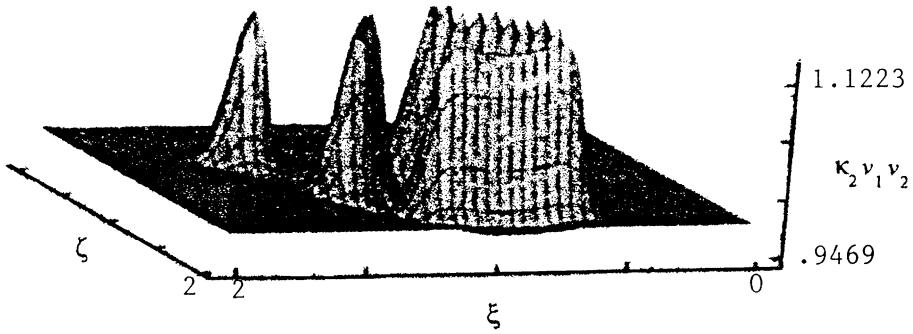

b. Elliptical Surface : (Semi major axis - 1. Semi minor axis -0.5)
Exposed Area 3.162 pi

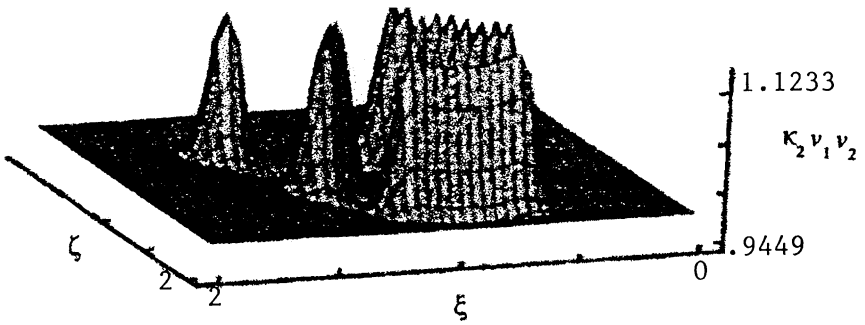

c. Cylindrical Surface : (Radius -1)
Exposed Area 2 pi

Fig. 7. Concentration profiles of $k_2 v_1 v_2$ for various surfaces (refer to data in Section 4).

Table 2
Maximum and minimum concentration values of v_1 and their location on the surface[a]

Surface	Maximum			Minimum			$(v_1)_{max} - (v_1)_{min}$
	ζ or K	ξ or I	v_1	ζ or K	ξ or I	v_1	Δv_1
Flat	1	1	0.00592895	14	18	0.00430282	0.00162613
Elliptical	41	42	0.00592917	15	17	0.00413956	0.00178960
Circular	4	3	0.00592950	13	14	0.00399391	0.00193559

[a] $\kappa_1 = \kappa_1 = 2000.0$, $\beta_{10} = 3.0$, $\beta_{20} = 10.0$, $\chi = 10.0$, $\tau = 1$.

Table 3
Maximum and minimum concentration values of v_2 and their location on the surface[a]

Surface	Maximum			Minimum			$(v_2)_{max} - (v_2)_{min}$
	ζ or K	ξ or I	v_2	ζ or K	ξ or I	v_2	Δv_2
Flat	18	33	0.1286840	1	1	0.08233350	0.0463505
Elliptical	14	18	0.1341670	43	39	0.08233320	0.0518338
Circular	14	18	0.1390320	2	4	0.08233280	0.0566992

[a] $\kappa_1 = \kappa_2 = 2000.0,\ \beta_{10} = 3.0,\ \beta_{20} = 10.0,\ \chi = 10.0,\ \tau = 1.$

Table 4
Maximum and minimum concentration values of $k_2 v_1 v_2$ and their location on the surface[a]

Surface	Maximum			Minimum			$(\kappa_2 v_1 v_2)_{max} - (\kappa_2 v_1 v_2)_{min}$
	ζ or K	ξ or I	$\kappa_2 v_1 v_2$	ζ or K	ξ or I	$\kappa_2 v_1 v_2$	$\Delta(\kappa_2 v_1 v_2)$
Flat	27	23	1.117560	19	21	0.9498360	0.167724
Elliptical	27	23	1.122250	16	18	0.9469120	0.175838
Circular	27	23	1.123290	15	28	0.9449950	0.178295

[a] $\kappa_1 = \kappa_2 = 2000.0,\ \beta_{10} = 3.0,\ \beta_{20} = 10.0,\ \chi = 10.0,\ \tau = 1.$

finite curvature versus a flat surface has an enhanced chemical activity contribution component due solely to the presence of surface curvature. If the surface curvature contributions to the catalyst surface activity is small when compared to the contribution of the surface irregularities, we can say with confidence that the contribution of surface curvature to the evaluation of φ can be neglected.

4. Conclusions

This paper describes the steady-state chemical performance of curved catalytic surfaces which are exposed to two species. The two main achievements of this paper are: (i) surfaces of arbitrary shapes can be considered. This aspect is important both from practical and theoretical view points. The coordinates in the generally curved surfaces are first generated numerically, and then the transformed conservation equations are solved using the generated coordinates. It must be emphasized here that even in the two curved surfaces considered in this paper, viz., circular and elliptical cylinders, rather than using the polar or elliptic coordinates, the coordinates were generated numerically as shown in Figs. 1 and 2; (ii) it has been found that for a given set of defects the species concentrations on a curved surface are enhanced over its flat surface counterpart. With the normalized species concentrations for the different surfaces being of the same order of magnitude, all the digits are significant from the point of view that the evidence of the surface curvature affecting the catalytic activity is noted in the thousandths or smaller decimal place value.

Acknowledgements

The authors gratefully acknowledge the financial support for this research received from the Hearin Educational Enhancement Fund (No. 305726-06100-021000) at the College of Engineering, Mississippi State University. This fund was generously provided as a grant from the Robert M. Hearin Foundation, Mr. Matt Holleman Trustee.

Appendix A. Laplacian in E^3 and its evaluation on a surface

Let x^i be a general coordinate systems. Referring to Warsi [14], the Laplacian of a function φ in terms of the coordinates x^i is given as

$$\nabla^2\varphi = g^{ij}\left(\frac{\partial^2\varphi}{\partial x^i \partial x^j} - \Gamma^r_{ij}\frac{\partial\varphi}{\partial x^r}\right) \tag{A.1}$$

where repeated indices imply summation from 1 to 3. Writing $x^1 = \xi, x^2 = \eta, x^3 = \zeta$ and denoting the partial derivatives by variable subscripts, we have

$$\begin{aligned} g\nabla^2\varphi = {} & G_1\varphi_{\xi\xi} + G_2\varphi_{\eta\eta} + G_3\varphi_{\zeta\zeta} + 2G_4\varphi_{\xi\eta} + 2G_5\varphi_{\xi\zeta} \\ & + 2G_6\varphi_{\eta\zeta} - G_1(\Gamma^1_{11}\varphi_\xi + \Gamma^2_{11}\varphi_\eta + \Gamma^3_{11}\varphi_\zeta) \\ & - G_2(\Gamma^1_{22}\varphi_\xi + \Gamma^2_{22}\varphi_\eta + \Gamma^3_{22}\varphi_\zeta) \\ & - G_3(\Gamma^1_{33}\varphi_\xi + \Gamma^2_{33}\varphi_\eta + \Gamma^3_{33}\varphi_\zeta) \\ & - 2G_4(\Gamma^1_{12}\varphi_\xi + \Gamma^2_{12}\varphi_\eta + \Gamma^3_{12}\varphi_\zeta) \\ & - 2G_5(\Gamma^1_{13}\varphi_\xi + \Gamma^2_{13}\varphi_\eta + \Gamma^3_{13}\varphi_\zeta) \\ & - 2G_6(\Gamma^1_{23}\varphi_\xi + \Gamma^2_{23}\varphi_\eta + \Gamma^3_{23}\varphi_\zeta) \end{aligned} \tag{A.2}$$

where Γ^i_{jk} are the Christoffel symbols of the second kind and are available in fully expanded form in [14]. Further, g_{ij} are the covariant metric coefficients, $g = det(g_{ij})$ and

$$\begin{aligned} & G_1 = g_{22}g_{33} - (g_{23})^2, \qquad G_2 = g_{11}g_{33} - (g_{13})^2, \\ & G_3 = g_{11}g_{22} - (g_{12})^2, \qquad G_4 = g_{13}g_{23} - g_{12}g_{33}, \\ & G_5 = g_{12}g_{23} - g_{13}g_{22}, \qquad G_6 = g_{12}g_{13} - g_{23}g_{11} \\ & g = g_{33}G_3 + g_{13}G_5 + g_{23}G_6 \end{aligned} \tag{A.3}$$

Consider a surface S embedded in E^3 and defined by $\eta = \eta_0 = \text{const.}$, on which the current coordinates are ζ and ξ. Thus, the function φ at S is a function of ζ and ξ but, in general, the derivative of φ with respect to η at $\eta = \eta_0$ are not zero. Without any loss of generality we take ζ and ξ as a general coordinate system in the surface and η as the transverse straight normal to the surface. Thus, $g_{12} = g_{23} = 0$ and $g_{22} = 1$. With this choice of coordinates

$$G_1 = g_{33}, \qquad G_2 = g_{11}g_{33} - (g_{13})^2, \qquad G_3 = g_{11},$$
$$G_4 = 0, \qquad G_5 = -g_{13}, \qquad G_6 = 0,$$
$$g = g_{11}g_{33} - (g_{13})^2 \tag{A.4}$$

Thus, Eq. (A.2) evaluated at $\eta = \eta_0$ gives

$$\nabla^2\varphi\Big|_{\eta=\eta_0} = \Delta_2\varphi + \varphi_\eta\big|_{\eta=\eta_0} + \frac{1}{2G_2}\frac{\partial G_2}{\partial\eta}\varphi_\eta\Big|_{\eta=\eta_0} \tag{A.5}$$

where $\Delta_2\varphi$ is the Beltramian of φ and Δ_2 is a surface operator defined as

$$\Delta_2 = g^{\alpha\beta}\left(\frac{\partial^2}{\partial x^\alpha \partial x^\beta} - Y^\delta_{\alpha\beta}\frac{\partial}{\partial x^\delta}\right) \tag{A.6}$$

where the Greek indices assume values 1 and 3, with repeated indices implying summation, and $Y^\delta_{\alpha\beta}$ are the surface Christoffel symbols, cf. Warsi [10,14]. Operating Eq. (A.6) on φ, we have

$$\Delta_2\varphi = \frac{1}{G_2}(g_{11}\varphi_{\zeta\zeta} - 2g_{13}\varphi_{\xi\zeta} + g_{33}\varphi_{\xi\xi}) + (\Delta_2\zeta)\varphi_\zeta + (\Delta_2\xi)\varphi_\xi \tag{A.7}$$

References

[1] F.F. Grinstein, H. Rabitz, A. Askar, J. Chem. Phys. 82 (1985) 3430.
[2] E.W. Thiele, Ind. Eng. Chem. 31 (7) 916–920.
[3] H. Hopster, H. Ibach, Surf. Sci. 77 (1978) 109.
[4] M.R. McClellan, J.L. Gland, F.R. McFeeley, Surf. Sci. 112 (1981) 63.
[5] G.A. Somorjai, Surf. Sci. 299/300 (1994) 849–866.
[6] C.K. Lee, S.L. Lee, Surf. Sci. 339 (1995) 171–181.
[7] J.A. Serri, J.C. Tully, M.J. Cardillo, J. Chem. Phys. 79 (1983) 1530.
[8] R.I. Cukier, J. Chem. Phys. 79 (1983) 2430.
[9] J.F. Thompson, Z.U.A. Warsi, C.W. Mastin, Numerical Grid Generation: Foundations and Applications, North-Holland, Amsterdam, 1985.
[10] Z.U.A. Warsi, J. Comput. Phys. 64 (1986) 82.
[11] E.S. Oran, J.P. Boris, Numerical Simulation of Reactive Flow, Elsevier Science, New York, 1987.
[12] W.R. Paterson, D.L. Creswell, Chem. Eng. Sci. 26 (1971) 605–616.
[13] P.A. Ramachandran, E.K.T. Kam, R. Hughes, Chem. Eng. Sci. 31 (1976) 244–247.
[14] Z.U.A. Warsi, Fluid Dynamics: Theoretical and Computational Approaches, 2nd Edition, CRC Press, Boca Raton, FL, 1998.